

Supplementary Material

for

Angiopoietin receptor TEK mutations underlie primary congenital glaucoma with variable expressivity

Tomokazu Souma, Stuart W. Tompson, Benjamin R. Thomson, Owen M. Siggs,
Krishnakumar Kizhatil, Shinji Yamaguchi, Liang Feng, Vachiranee Limviphuvadh,
Kristina N. Whisenhunt, Sebastian Maurer-Stroh, Tammy L. Yanovitch, Luba Kalaydjieva,
Dimitar N. Azmanov, Simone Finzi, Lucia Mauri, Shahrbanou Javadiyan, Emmanuelle Souzeau,
Tiger Zhou, Alex W. Hewitt, Bethany Koss, Kathryn P. Burdon, David A. Mackey, Keri F. Allen,
Jonathan B. Ruddle, Sing-Hui Lim, Steve Rozen, Khanh-Nhat Tran-Viet, Xiaorong Liu,
Simon John, Janey L. Wiggs, Francesca Pasutto, Jamie E. Craig, Jing Jin, Susan E. Quaggin and
Terri L. Young

Supplementary Methods

Human study participants and DNA extraction

Subjects and their families were recruited from multiple international centers, for which each site received study approval from their respective Institutional Review Board (IRB). These studies adhered to the tenets of the Declaration of Helsinki. The IRBs approved the recruitment of individuals and family members with inherited developmental ophthalmologic disorders, the collection of blood, cheek cells and saliva samples for DNA extraction, screening for genetic mutations and creation of genotype-phenotype correlations. Written informed consent for study participation was obtained from the subject or subject's parents, as appropriate. The studies were also compliant with the Health Insurance Portability and Accountability Act (HIPAA).

Primary congenital glaucoma (PCG) was defined by the following characteristics: *(i)* age of onset less than 3 years, *(ii)* increased corneal diameter greater than 10 mm accompanied by corneal edema and/or Haab striae and *(iii)* increased IOP greater than 21 mmHg and/or optic nerve cupping greater than 0.4. Any patient with other ocular abnormalities or systemic condition, other than iris stromal hypoplasia, was excluded from the study. Ocular anomalies excluded were posterior embryotoxon, correctopia, cataract, Axenfeld Reiger syndrome, Peter's Anomaly, apparent corneal dystrophy, megalocornea, and aniridia. A questionnaire request for family and medical history was completed by the subject and/or the subject's parent or guardian.

In total, 189 families were included in the study. All families had been previously screened for known PCG gene variants and found to be negative. One-hundred and seventy-three of the families contained only a single affected individual, 13 families contained 2 affected individuals, 2 families contained 3 affected individuals and 1 family included 4 affected

individuals (1 affected by family history, 2 were later-onset disease). One-hundred and forty of the affected individuals showed disease in both eyes, 34 were unilaterally affected and 35 were unknown. Blood, buccal cheek or saliva samples were collected from the subject and any available family members. Genomic DNA was extracted according to the manufacturer's instructions using AutoPure LS DNA Extractor (QIAGEN Inc., Valencia, CA) and PUREGENE reagents (Gentra Systems Inc., Minneapolis, MN).

Exome sequencing and *TEK* Sanger sequencing

For the initial U.S. exome sequencing cohort, 21 affected individuals from 20 families underwent exome sequencing using the NimbleGen v2 exome capture kit (Roche NimbleGen, Inc., Madison, WI) and HiSeq2000 platform (Illumina, Inc., San Diego, CA). Raw sequence reads were aligned to the human reference genome assembly (GRCh37/hg19) using the Burrows-Wheeler Aligner (BWA) (1) and variants were called with the Genome Analysis Toolkit (GATK) (2, 3). Variants were analyzed and filtered using SNP and Variation Suite software (SVS version 8.3, Golden Helix, Inc., Bozeman, MT) and sequence reads were visualized using GenomeBrowse (Golden Helix, Inc., Bozeman, MT). All variants were validated by direct Sanger sequencing.

DNA samples from an additional 24 Italian families (74 exomes, 26 affected individuals) were enriched using the SureSelect Human All Exon Kit version 5 (Agilent, Santa Clara, CA) and paired-end sequenced (100 bp forward and reverse) on an Illumina HiSeq 2500 instrument (Illumina, San Diego, CA). Image analysis and base calling was performed using the HiSeq instrument control software with default parameters. After de-multiplexing with bcl2fastq v1.8.4 from Illumina, read alignment was performed with BWA (1, 2) version 0.7.8 using the

GRCh37/hg19 human reference genome assembly. Duplicate reads were marked with Picard MarkDuplicates (version 1.111, <http://broadinstitute.github.io/picard>). Furthermore, local re-alignment around potential insertion and deletion (indel) sites was performed with GATK version 3.1 (2, 3). Single-nucleotide variants and small indels were detected using five different caller algorithms: HaplotypeCaller and UnifiedGenotyper of the aforementioned Genome Analysis Toolkit (2, 3), SNVer (4), freeBayes (<http://arxiv.org/abs/1207.3907v2>), and Platypus (5). Variant annotation was performed using ANNOVAR (6) in conjunction with a variety of open and proprietary annotation database files. Detected variants were confirmed by direct Sanger sequencing using the primers listed in **Supplemental Table 1**.

Exomes from a further 44 Australian families (44 affected individuals) were captured using the Agilent SureSelect v4 kit (Agilent, Santa Clara, CA), and sequenced on an Illumina HiSeq2500 (Illumina, San Diego, CA) (125bp paired-end library). Reads were aligned to the GRCh37/hg19 human reference genome using BWA, and duplicates were marked and removed using Picard (1, 2). Single nucleotide variants and indels were called using GATK and annotated against RefSeq transcripts using ANNOVAR (2-4, 6). Variants present in 84 unrelated non-glaucomatous control exomes were eliminated.

An additional 17 families (79 exomes, 31 affected individuals) collected in Boston, USA, were captured with the Agilent SureSelect V4+UTR+Mito Agilent exon capture (71.4 Mb target region) and sequenced on an Illumina HiSeq2500 (75X mean coverage). The sequence data was aligned using BWA (version 0.6.2-r126), duplicates were removed and variants called using SAMtools (version 0.1.18 or r982:295), which were then refined using a custom human bp codon resource (Genomics core, Mass Eye and Ear) as well as GATK. Custom scripts were also developed and used to annotate variants.

A further 84 families (87 affected individuals) from the USA, Bulgaria, Brazil, Australia, Italy and Romani population were screened for coding exon and splice site variants in *TEK* (NCBI Reference Sequence, NM_000459.4) by direct Sanger sequencing. In total 58 families (including 7 of 10 families that harbored a *TEK* mutation reported here) were screened for *TEK* core promoter variants (genomic sequence 60 bp upstream to 40 bp downstream of the predicted transcriptional start site at position chromosome 9:27,109,145 (GRCh37/hg19)). Genomic primer sequences are provided in **Supplemental Table 1**.

***In silico* functional studies**

Polymorphism Phenotyping version 2 (PolyPhen-2, <http://genetics.bwh.harvard.edu/pph2/>) (7, 8) and SIFT (Sorting Intolerant From Tolerant version 5.2.2, <http://sift.bii.a-star.edu.sg/>) (9) were used to predict any functional effects that the three *TEK* missense variants (p.C233Y, p.Y611C, and p.K294N) may have on protein function. Three versions of SIFT analyses were performed using different multiple alignments of homologous sequences as input. Alignments were created using MAFFT (version 7.130b) with L-INS-I parameters (10) and any sequences seen to contain large gaps in Jalview (version 2.8) (11) were removed. The first SIFT analysis used 73 orthologs of human *TEK* (NP_000450.2), retrieved using Orthologue search on ANNOTATOR (12). Since *TEK* belongs to the TIE receptor family that contains both *TEK* (TIE2) and TIE1, we wanted to know whether wild-type (WT) residues of the three missense variants were conserved throughout the whole family or subfamily-specific residues. Therefore, the second analysis incorporated an additional 80 TIE1 (NP_005415.1) orthologs for an analysis of 155 TIE receptor family sequences (which include human *TEK* and TIE1). Finally, a SIFT-BLink (http://sift.bii.a-star.edu.sg/www/SIFT_BLink_submit.html)

analysis was performed using 399 sequences closely related to TEK (obtained via BLAST, <http://blast.ncbi.nlm.nih.gov/Blast.cgi>).

To analyze the effect of missense variants on protein structure, FoldX (<http://foldx.crg.es/>, <http://foldxyasara.switchlab.org/>)(13) analyses were performed using known crystal structures when available. The crystal structures were retrieved from the PDB (14) (Protein Data Bank) database via BLAST search. For the p.C233Y and p.K294N variants, the human TEK (PDB ID: 2GY5(15); E-value=0.0, Resolution=2.9 Angstrom), was used for the FoldX analysis. For the p.Y611C variant, since the fibronectin domain structure of TEK was unavailable, the respective domain subsequence of TEK (543-625aa) was used to search the PDB for suitable templates using HHpred (<http://toolkit.tuebingen.mpg.de/hhpred>). A crystal structure of an internal FN3 domain from human Contactin-5 (PDB ID: 4N68 chain A (16)) was identified as the top-hit (E-value=1.2e-18 resolution=1.8 Angstrom) and used as a template structure for modeling with MODELLER (17) with loop refinement. The FoldX plugin for YASARA (18) was then used for differential stability analysis of wild-type and mutant versions of the above described structures and modeled with 5 repetitions each and visualized with YASARA (19). All three mutations were consistently found to be destabilizing, with a stronger effect estimated for the p.C233Y and p.Y611C mutations (see **Supplemental Figure 4** and **5**, and **Table 3**). When we looked at the subfamily-specific conservation at the variant's position and neighboring amino acids, p.C233 and p.Y611 were highly conserved throughout the TIE receptor family from human, primates, mouse, rat, chicken, frog and zebrafish (**Supplemental Figure 6**).

The nonsense mutation p.Y307* either results in transcript loss due to nonsense-mediated decay or causes truncation of TEK protein from the third EGF domain onwards, and should therefore have a strong effect because it lacks the entire intracellular protein

kinase domain (**Supplemental Figure 2A**). This domain is an important part of initiating downstream signaling, and our cellular functional studies have proven that the p.Y307* mutant cDNA does not produce an intact protein (**Figure 2A** and **Supplemental Figure 2B**). Another nonsense mutation, p.G984*, if escaping nonsense-mediated decay, causes disruption of the DFG motif in the activation loop of the kinase domain, as in our artificial kinase dead mutant (p.D982A), and truncation from the middle of the protein kinase domain (See **Supplemental Figure 2A**). We attempted to calculate the change in structural stability by modeling the p.G984* truncation using the human TEK kinase domain crystal structure (PDB ID: 2WQB (20)). The estimated free energy of the wild-type structure is 42.45 kcal/mol. However, when the region from 984 onwards is deleted, the energy is raised to 59.02 kcal/mol, which means the truncation strongly destabilizes the protein. The p.E150* and p.K745fs mutations are also expected to cause the loss of functional protein by either nonsense-mediated decay or protein truncation (See **Supplemental Figure 2A**).

For the two invariant splice donor variants (c.760+2T>C and c.3300+2delT), we used Human Splicing Finder version 3.0 (HSF, <http://www.umd.be/HSF3/HSF.html>) (21) and Automatic Analysis of SNP sites (AASsites, <http://genius.embnet.dkfz-heidelberg.de/menu/biounit/open-husar>) (22) to analyze whether the variants could cause changes to the splice sites. HSF utilizes two algorithms, which are position weight matrices (HSF Matrices) and maximum entropy (MaxEnt) to predict a mutation's effect on splicing motifs including donor splice sites. We used the gene name of “*TEK*” and mutants c.760+2T>C and c.3300+2delT as input, and selected the longest transcript (ENST00000380036) for the analysis. Both variants were predicted to result in a “Broken WT Donor site”, which means that the variants likely affect splicing (**Table 2**).

Similarly, AASsites is an automated bioinformatics pipeline to analyze SNP containing DNA sequences mainly for finding SNPs, which cause a change in the splicing pattern using different gene prediction programs. The results are combined, and a probability for a change in splicing in the classes "likely", "probable", and "unlikely" are given. Input DNA sequence of the c.760+2T>C and the c.3300+2delT variants were “TATGGGAAGGACGTGTGAGAAGGGCAAGTAAAGAGACTTGATAAGTAAG” and “ACAGAATGTTAGAGGAGCGAAAGGAAGTATTAAGTCAGGCAGGAGAT”, respectively, together with the EnSEMBL gene ID ENSG00000120156. Results of both variants were predicted to cause a “probable” change in splicing with the score 1 for SNP distance and gene prediction. Altogether, both HSF3 and AASsites programs agree that the variants c.760+2T>C and c.3300+2delT affect the splice sites. Furthermore, our cell-based exon trapping functional assays proved that these 2 splice donor variants led to the loss of normal functional protein (See **Supplemental Figure 3** and **Figure 4**).

Cloning of *TEK*-expressing plasmids

Full-length human *TEK* cDNA was cloned into vector pcDNA3.1 with the stop codon replaced by an in-frame Flag-tag sequence encoding DYKDDDDK using XbaI/ApaI sites using standard procedure. To introduce mutations to TEK-Flag expressing vector (p.D982A, p.Y307*, p.K294N, p.C233Y, and p.C224S), site-directed mutagenesis was performed using Primestar Max (Takara, Japan), and sequence validated. To make the deletion mutants, synthesized DNA was sub-cloned into wild type TEK-Flag plasmid using BamHI site and sequence verified. Please see **Supplemental Figure 7** for details.

Soluble TEK detection assay

TEK expressing vectors that encode cDNA for TEK306-Fc (expected product of p.Y307*) or TEK440-Fc fusion protein were constructed (**Supplemental Figure 7**), and transfected to HEK293 cells. C-tail Fc-tag allows the protein to be pulled down by protein G beads and to be detected by anti-human Fc antibody (1:5K, cat. 31413, Invitrogen). Secreted TEK-Fc fusion protein into the serum free medium was purified by protein G Sepharose beads (GE healthcare), and extracted by 2x sample buffer. TEK-Fc fusion protein was detected by immunoblotting with anti-human Fc antibody. As TEK440-Fc fusion protein was reported to secrete into the medium, this artificial fusion protein was used as the positive control (23).

Western blot analysis

Plasmids (2.5µg) containing variant or wild type TEK-Flag were transfected into sub-confluent HEK293 cells in 6 well dishes using lipofectamine 2000 (Life Technologies, Carlsbad, CA). Two days after transfection, cells were harvested by NP40 buffer with proteasomal inhibitor cocktail (Sigma-Aldrich, St. Louis, MO) and phosphatase inhibitor cocktail (Sigma-Aldrich), with addition of NaOV₃, NaF₂, and PMSF. For immunoprecipitation, TEK-Flag protein in supernatant was immunoprecipitated using anti-Flag antibody-conjugated beads (cat. A2220, Sigma-Aldrich) for 2 hrs at 4°C. Immunoprecipitated proteins were then washed with Tris-balanced saline buffer with Triton X100 (0.1%, TBST) three times, and eluted with 2x sample buffer. Same volume of each sample was used to detect total phosphorylation level and protein expression level by using anti-pY antibody (1:10K, 4G10P, cat. 05-1050X, EMD Millipore, Billerica, MA) and anti-Flag M2 antibody (1:10K, clone M2, cat. F3165, Sigma-Aldrich) by immunoblotting after separation with SDS-PAGE and transferred to PVDF

(polyvinylidene difluoride) membrane. For detecting the subcellular localization of TEK proteins, cell lysates were separated into supernatant soluble fraction and insoluble pellets. 4x sample buffer was added to the supernatant. Insoluble proteins in pellets were washed twice with TBST, and extracted using 2x sample buffer and sonicated. The same amounts of samples were subjected to SDS-PAGE and transferred to PVDF membrane. The Flag signal was detected using anti-Flag M2 antibody (Sigma-Aldrich). For loading control, α -tubulin in soluble fraction was detected using anti- α -tubulin antibody (Clone DM1A, cat. 32293, Santa Cruz, Dallas, TX). For the proteasomal inhibitor study, transfected HEK293 cells were treated with 5 μ M MG132 (Enzo Life Science, Farmingdale, NY) or DMSO for indicated times. Cell lysates were fractionated and immunoblotted as described above.

Stable isotope labeling by amino acids in cell culture (SILAC)

SILAC analyses were performed as previously described (24). HEK293 cells were grown in the culture medium with light form of isotopes (Arginine 0, Lysine 0) or heavy form of isotopes (arginine 10, lysine 8) in 10 cm dishes, and allowed more than 5 cell doublings for complete labeling (confirmed by Liquid chromatography-tandem mass spectrometry, LC/MS/MS, data are not shown). After cells fully incorporated heavy amino acids, cells were transfected with 20 μ g TEK-Flag plasmids expressing wild type (WT) or variants using lipofectamine 2000. WT-TEK-Flag vector was transfected to light-labeled cells and variants were transfected to heavy-labeled cells, thereby WT TEK was labeled by light, and variants were labeled by heavy isotope. Then, cells were harvested with NP40 buffer. Cell lysates were centrifuged and the supernatants from heavy (variants) and light (WT) were mixed together, and immunoprecipitated with anti-Flag conjugated beads (Sigma). Immunoprecipitated proteins were eluted with 2x

sample buffer. Samples were separated by SDS-PAGE, and stained with blue dye (Thermo Scientific, Waltham, MA). Corresponding gel pieces for TEK-Flag proteins were excised, and then subjected to in-gel-digestion with trypsin. Digested peptides were analyzed with LC/MS/MS.

Mass spectrometry

The extracted peptides were loaded directly onto a 15 cm long, 75 μ M reversed phase capillary column (ProteoPepII C18, 300 Å, 5 μ m size, New Objective, Woburn MA) and separated with a 200-minute gradient from 5% acetonitrile to 100% acetonitrile on a Proxeon Easy n-LC II (Thermo Scientific). The peptides were directly eluted into an LTQ Orbitrap Velos mass spectrometer (Thermo Scientific) with electrospray ionization at 350 nl/minute flow rate. The mass spectrometer was operated in data dependent mode, and for each MS1 precursor ion scan, the ten most intense ions were selected from fragmentation by CID (collision induced dissociation). The other parameters for mass spectrometry analysis were: resolution of MS1 was set to 60,000, normalized collision energy to 35%, activation time to 10 ms, isolation width to 1.5, and rejection of +4 and higher charge states. Data was processed with Proteome Discoverer (version 1.4; Thermo Scientific, San Jose, CA), using the embedded SEQUEST HT search engine. The data were searched against human reference proteome (Proteome ID: UP000005640, Download date: February 2015) (uniprot.org). The other parameters were as follows: (i) enzyme specificity: trypsin, with maximum of two cleavages; (ii) variable modification: methionine oxidation and cysteine carboamidomethylation; (iii) serine, tyrosine and threonine phosphorylation; (iv) SILAC labels, lysine (13C6 lysine and arginine (+6 Da), 13C6 15N2 lysine (+8 Da) and 13C8 15N2 arginine (+10 Da); (v) precursor mass tolerance was \pm 10 ppm; and (vi)

fragment ion mass tolerance was ± 0.8 Da. All spectra were searched against target/decoy databases, and the results were used to estimate the q values in Percolator algorithm as embedded in Proteome discoverer 1.4. The peptide identification was considered valid at q value < 0.1 and was grouped for protein inference to satisfy the rule of parsimony. The confidence on phosphorylation for each site was calculated by PhosphoRS node and the ratio of light to heavy peptide was calculated by quantification node in Proteome discoverer. The ratio was normalized by the protein abundance for analyzing phosphorylation status. For peptide level validation, we choose a 1.5 fold threshold as indicative of an increase and a 0.5 threshold as a reduction. Furthermore, all phosphorylated assignments demonstrating significant differences were manually validated.

TEK localization assay

HUVECs obtained from ATCC were cultured using EndoGRO LS Supplement Kit (EMD Milipore). Cells were transfected with either wild type or variant TEK-Flag vector by electroporation with 4D nucleofector (Lonza, Basel, Switzerland). The transfected cells were then grown on glass cover slips coated with 0.1% poly L-lysine (Sigma-Aldrich). Cells were stimulated with recombinant human Angiopoietin 1 (600 ng/mL, R and D systems, Minneapolis, MN) for 30 min at 37°C (25, 26), and then fixed with 2% paraformaldehyde (PFA) for 15 min at room temperature. Cells were made permeable with 0.1% Triton X100 in PBS for 10 min and were blocked with 1% bovine serum albumin/ phosphate balanced saline (PBS) for 30 minutes, and incubated with primary antibody against Flag (M2, 1:100, Sigma-Aldrich) and against ZO-1 (1:200, cat. 402200, Invitrogen) overnight at 4°C. Then, Alexa 488- or Alexa 555-conjugated secondary antibodies (Cat. A-11029 and A-21433, Life technologies) were used to detect Flag or

ZO-1 signals. 4',6-Diamidino-2-Phenylindole dihydrochloride (DAPI) was used for staining nuclei. Images were obtained using Nikon C2+ confocal microscopy.

Exon trapping splicing assay

Phusion Hot Start High-Fidelity DNA polymerase (Thermo Fisher) was used to amplify 1457bp and 831bp genomic DNA fragments containing *TEK* exons 5-6 and exon 22, respectively, from affected individuals from families 7 and 8 and a control subject. PCR products were inserted into the multiple cloning site of the exon trapping vector, pSPL3 (Invitrogen-Life Technologies, discontinued), using XhoI and BamHI endonucleases (Life Technologies) and the resulting constructs were verified by Sanger sequencing. Wild-type (WT) and mutant (M) mini-genes were transfected into Cos-7 cells using FuGene 6 (Stratagene, La Jolla, CA), and 24 hours later total RNA was isolated using the RNeasy Mini Kit (QIAGEN Inc.). A High Capacity cDNA Reverse Transcription Kit (Applied Biosystems, Foster City, CA) was used with random primers to generate cDNA, and the splicing vector-transcribed cDNA species were specifically amplified by PCR using primer pairs corresponding to sequences in vector exons V1 and V2. The resulting RT-PCR products from the wild-type and mutant mini-genes were visualized by gel electrophoresis and their sequence composition determined by Sanger sequencing.

Mice and breeding

All animal experiments were approved by the Animal Care Committee at the Center for Comparative Medicine of Northwestern University (Evanston, Illinois, USA). Whole-body *Tek* conditional knockout mice were bred and maintained as previously described (27). *Tek* wild-type, hemizygous, and homozygous knockout mice were generated by crossing *Tek*^{COIN/WT};*ROSA26-rtTA*;*tetO-Cre* males with hemizygous *Tek* knockout females (*Tek*^{Δ/WT};*ROSA26-rtTA*;*tetO-Cre*). Doxycycline hyclate (5%, Sigma-Aldrich) was added to the drinking water of pregnant dams from 17.5 days post *coitum* (17.5 d.p.c.) to induce *Tek* deletion until postnatal day (P) 7. For the present study only *Tek*^{WT/WT} (control), *Tek*^{Del/WT} (hemizygote; *Tek*^{+/-} in **Figure 5 – 7**), and *Tek*^{Del/COINΔE17.5} (knockout; *Tek* cKO in **Figure 5 – 7**) mice were included in experimental groups (**Supplemental Figure 12**). Primers used for genotyping are listed in **Supplemental Table 2**. TEK expression in lung lysates was analyzed by standard blotting procedures using anti-TEK antibody (1:1000, sc-324, Santa Cruz).

Intraocular pressure measurement

Intraocular pressure was measured at 4 to 25 weeks of age using a Tonolab rebound tonometer (iCare, Vantaa, Finland) as previously described (27, 28). Mice were restrained in a soft plastic cone, and IOP measurements from each eye were averaged from 3 sets of 6 recordings. Littermate controls were used for all live-animal studies.

Schlemm's canal imaging

Schlemm's canal imaging was performed as previously described (27). Eyes from 10 to 25 week-old control, *Tek*^{+/-}, and *Tek* cKO mice were enucleated and immersion fixed by Periodate-lysine-paraformaldehyde (29). After fixation, a single incision was made from the optic nerve to the center of the cornea. The lens, retina and iris were removed, and the remaining eye tissues were stained for immunofluorescence imaging using standard protocols. After blocking, (5% donkey serum, 5% bovine serum albumen (w/v), 0.5% Triton X100 in TBS, pH 7.4) eyes were incubated in appropriate primary (Rat anti-CD31, clone MEC13.3, cat. 553370, BD Pharmingen, San Jose, CA) and fluorescently labeled secondary antibodies (Invitrogen, Carlsbad, California) diluted in blocking buffer. To allow flat-mounting, a series of incisions were made in the cornea and sclera before the eyes were extended, mounted and imaged using a Nikon C2+ confocal microscope. For low-magnification images of Schlemm's canal morphology, the confocal pinhole was set to 150 μ m, and a series of stitched images was captured using a 20x objective. Depth projections were prepared from confocal Z-stacks captured using a 20x objective and 20 μ m pinhole (1.2 airy units). As Schlemm's canal is absent in *Tek* knockout mice, the superficial limbal vasculature was used for orientation. The imaging plane was focused on the superficial limbal vasculature and 44 μ m Z-stacks towards the center of the eye were captured. Fiji software was used to depth-code slices, and pseudo-colored 3D projections were prepared (30).

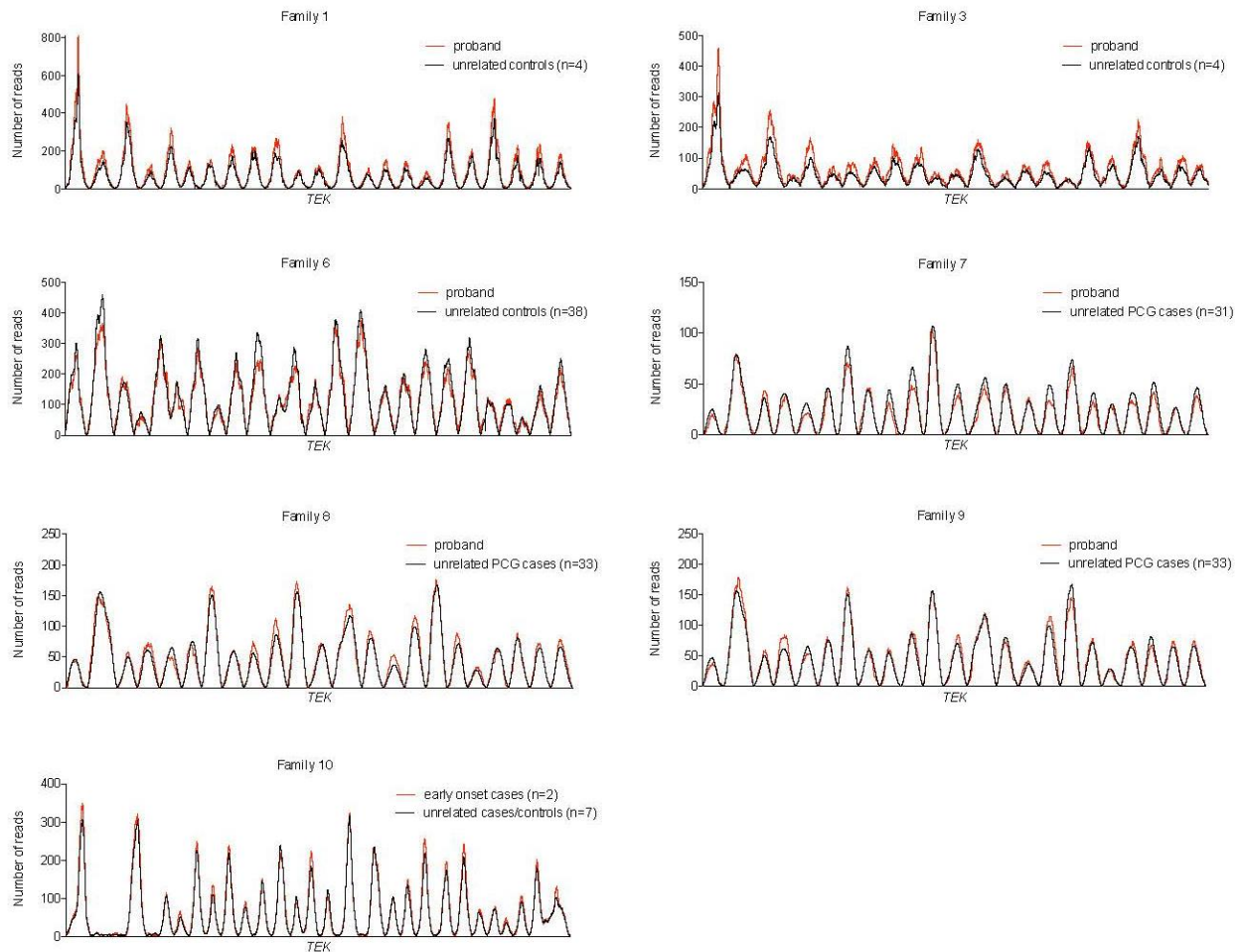
Quantitative analysis of SC morphology

Flat-mounted eyes from wild-type and *Tek*^{+/-} mice were stained with anti-CD31 antibody to visualize SC and images were captured by using a Nikon C2+ confocal microscope as described above. Blinded observers counted the number of narrowing points in the full length SC as shown in **Figure 6** (17 eyes for *Tek* ^{+/+} and 23 eyes for *Tek* ^{+/-}; 10 to 25 week-old mice, littermate controls were used).

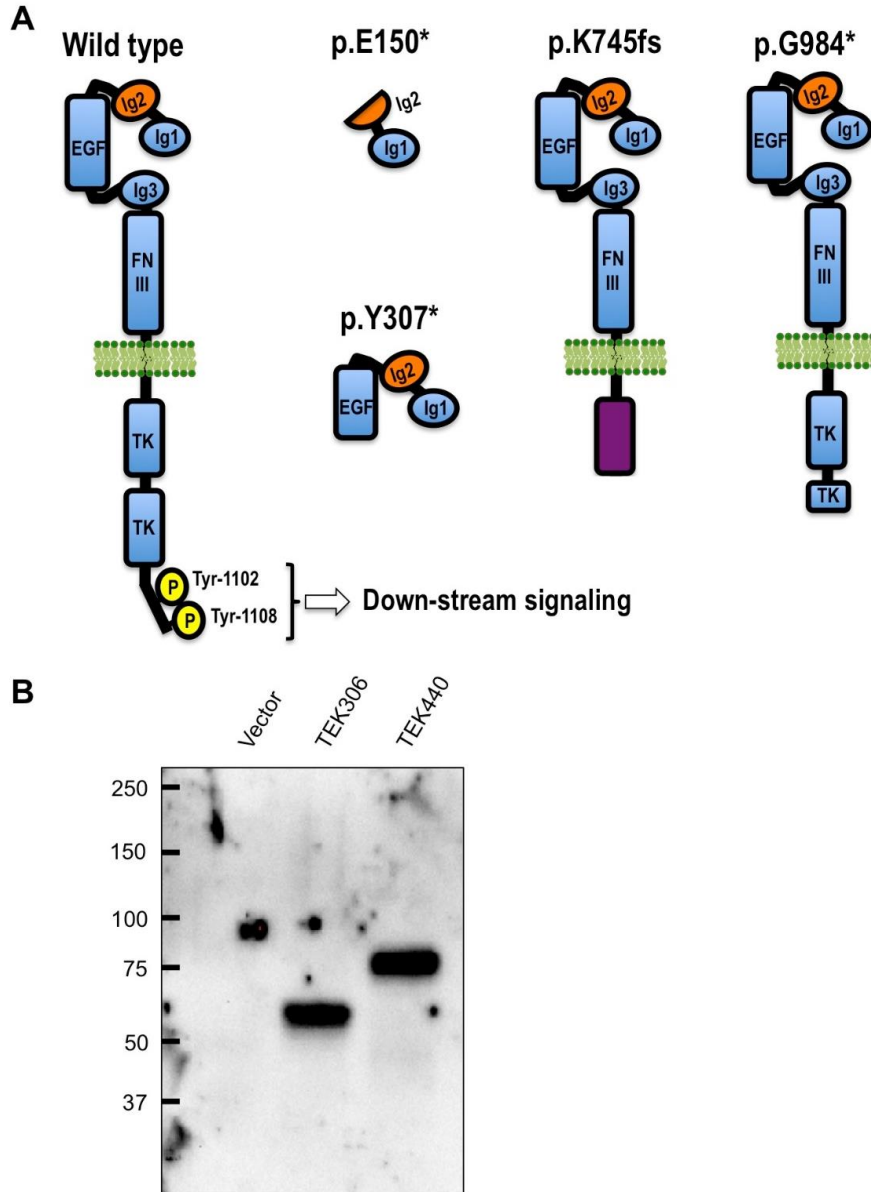
Histological analysis for iridocorneal angle of eyes

Eyes were enucleated and fixed in Smith Rudt fixative for 24 hrs, then transferred to 0.1M Phosphate Buffer and processed as described before (31-33). Briefly, samples were placed and processed in a 20ml glass vial (one sample/vial) and subjected to dehydration using an ethanol series on a rotator at room temperature (70% ETOH for 2 hours, 95% ETOH for 1 hour on rotator at RT and 95% ETOH). The Technovit 7100 Glycol Methacrylate Kit is used for infiltration and embedding (Energy Beam Sciences, Catalog # H7100). Eyes are embedded in a mold and the orientation noted. 18-42 section of 2 μ m thickness were cut from three different locations of each eye as described before (31). After hematoxylin eosin staining the eye were imaged using Nanozoomer slide scanner (Hamamatsu Photonics). The images were then visually analyzed blindly for pathological changes. Based on our experience at looking at over 40 wild mice with mixed background we assessed if the iridocorneal angle, the trabecular meshwork and the Schlemm's canal had a normal appearance. Conclusions were drawn only from high quality sections and abnormalities had to be present in multiple sections from the same region to be regarded as real.

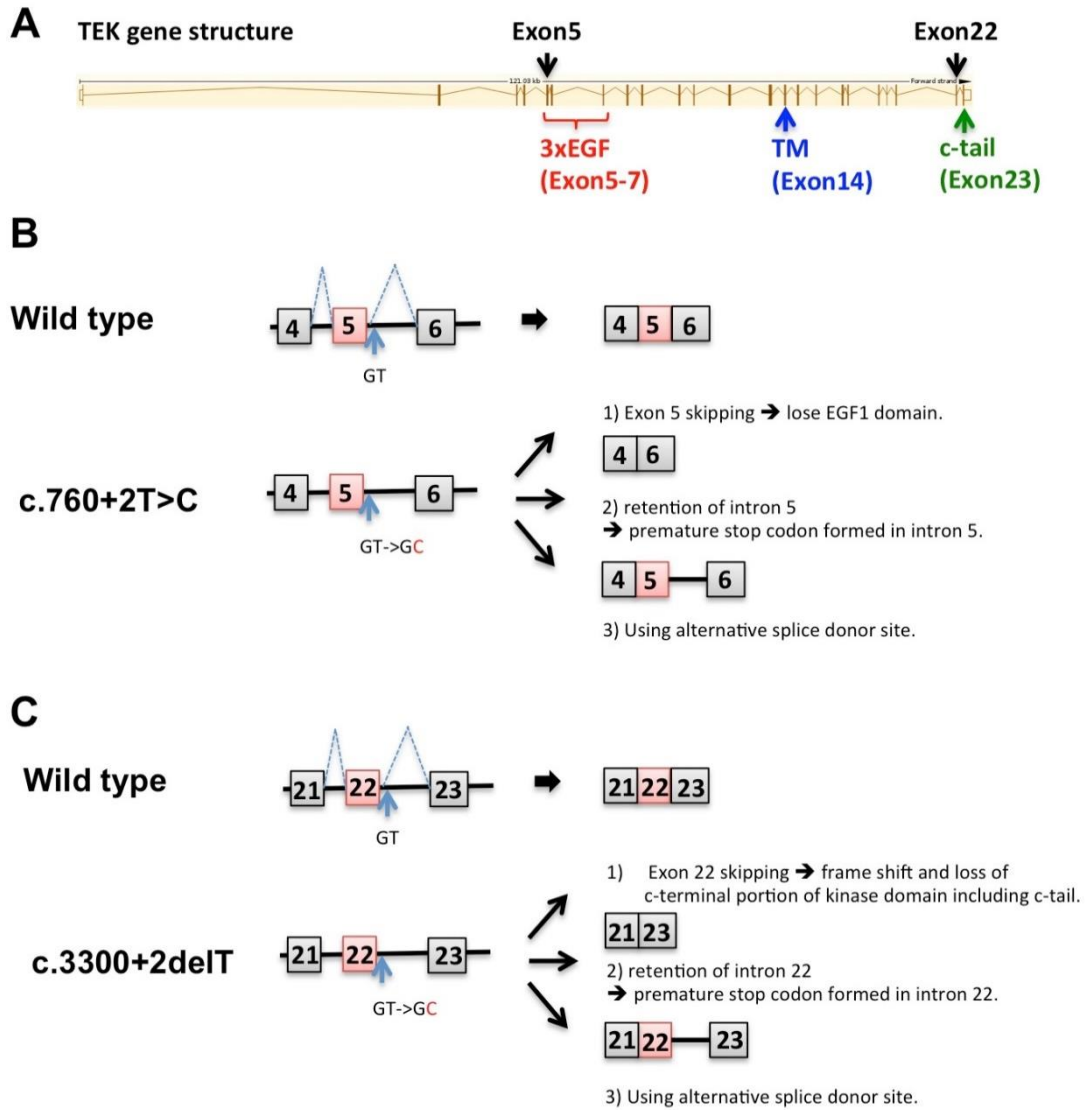
Supplemental Figures



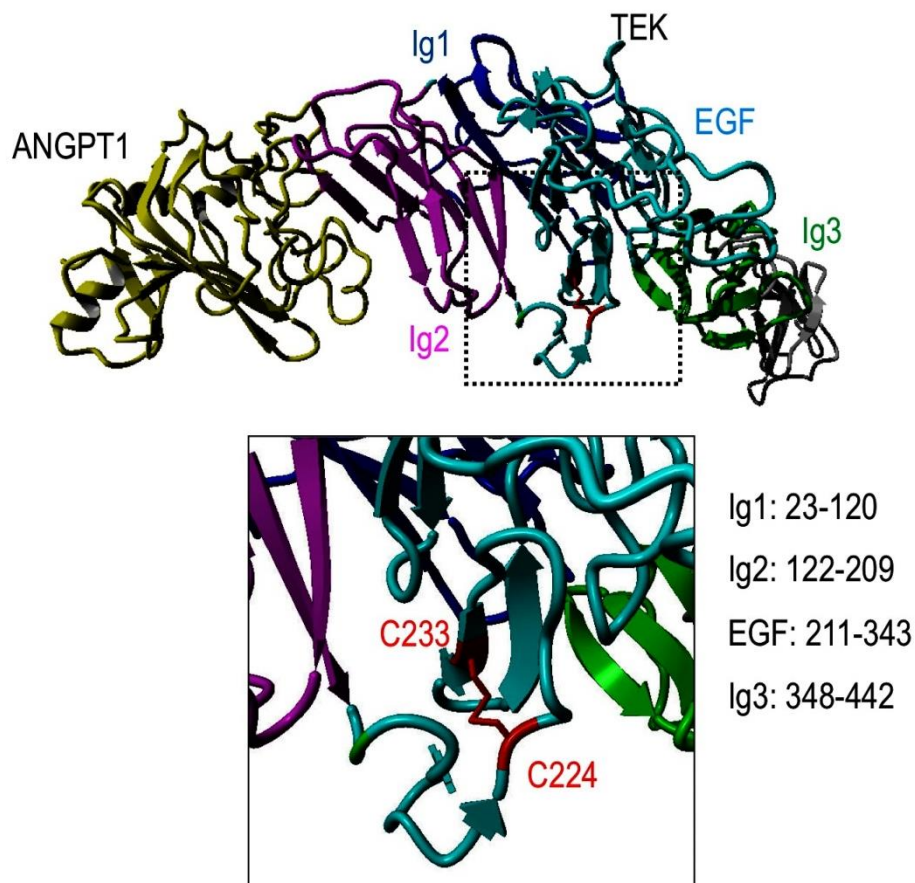
Supplemental Figure 1. Copy number variant (CNV) analyses using whole exome sequence (WES) read depths. Read depth coverage is shown for the *TEK* exons (individual peaks) obtained from a single PCG case (red line) and compared to the average read depth obtained from unrelated samples exome sequenced in the same batch (black line). By this method, *TEK* CNVs were not detected in all 7 WES families known to contain a single nucleotide variant in *TEK*. Please note that mutation screening of the *TEK* gene in families 2 (p.T19_R210del), 4 (p.K294N), and 5 (p.Y611C) was performed by direct Sanger sequencing.



Supplemental Figure 2. Predicted TEK mutant protein structures. (A) Schematic diagrams of TEK mutants harboring either nonsense mutations or a frame-shift mutation are shown. All the predicted proteins lack an intracellular signaling domain, making all the mutant alleles functionally null. Furthermore, most mRNA with premature termination is predicted to undergo mRNA degradation via nonsense-mediated decay. (B) Detection of secreted TEK mutant protein. The p.Y307* mutant cDNA with C-tail Fc-tag was expressed in HEK293 cells (TEK306: See Supplemental Figure 7 for the constructs). The secreted protein, TEK306-Fc, in the medium was detected by anti-human Fc antibody. The TEK440-Fc artificial protein was used as a positive control, as previously reported (23). Data representative of 3 biological replicates are shown.

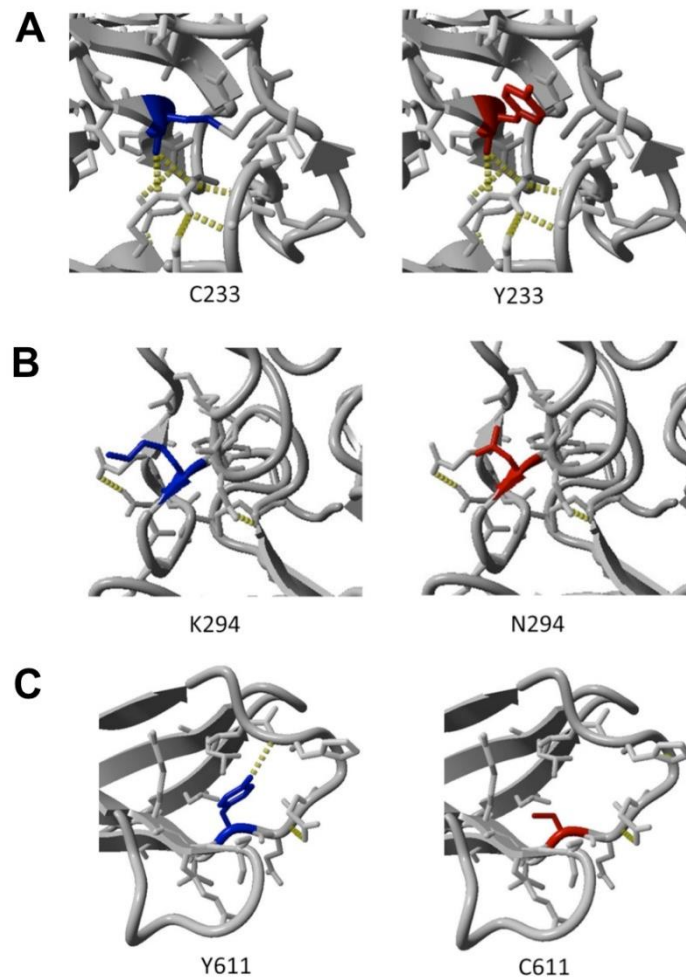


Supplemental Figure 3. Predicted effects of splice donor site mutations. Schematic diagrams of *TEK* mutants harboring invariant splice donor site mutation are shown. (A) *TEK* gene structure. Exon 5 encodes the EGF1 domain and exon 22 encodes a part of the C-terminal kinase domain. (B) Splicing predictions for the c.760+2T>C mutation in Family 7. (C) Splicing predictions for the c.3300+2delT mutation in Family 8. TM, transmembrane domain.

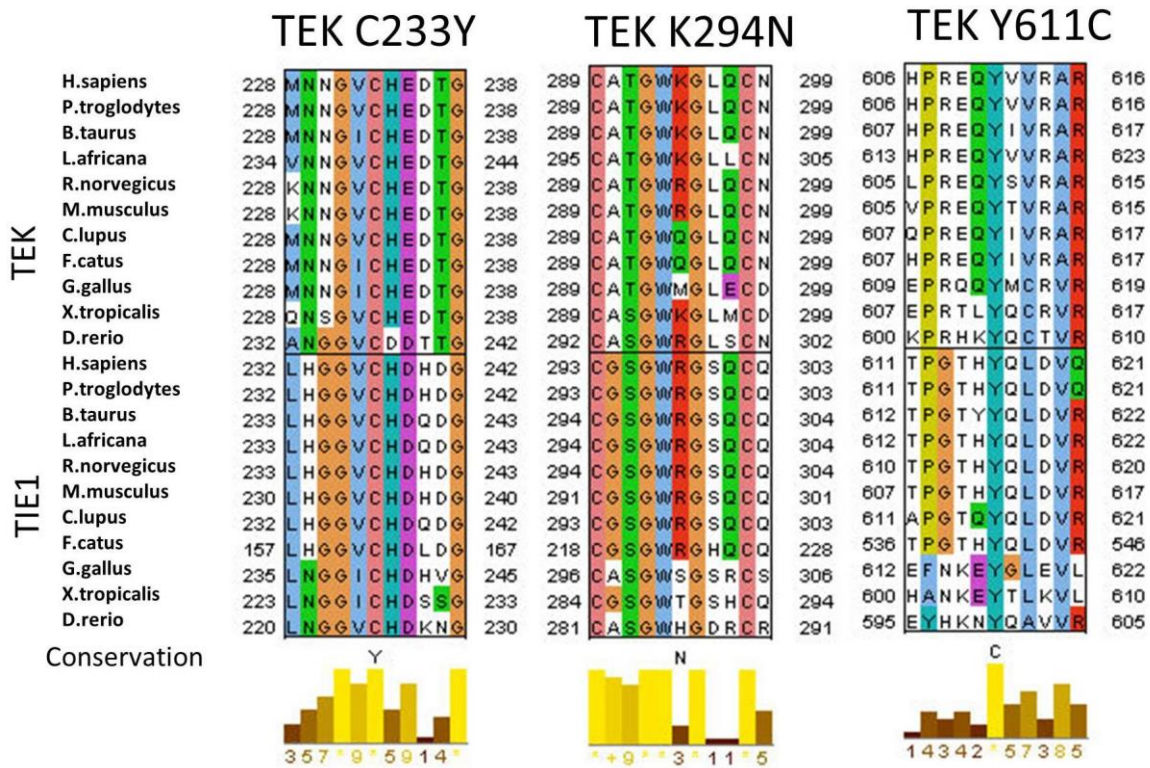


Supplemental Figure 4. C233 and C224 form a disulfide bond within the EGF1 domain.

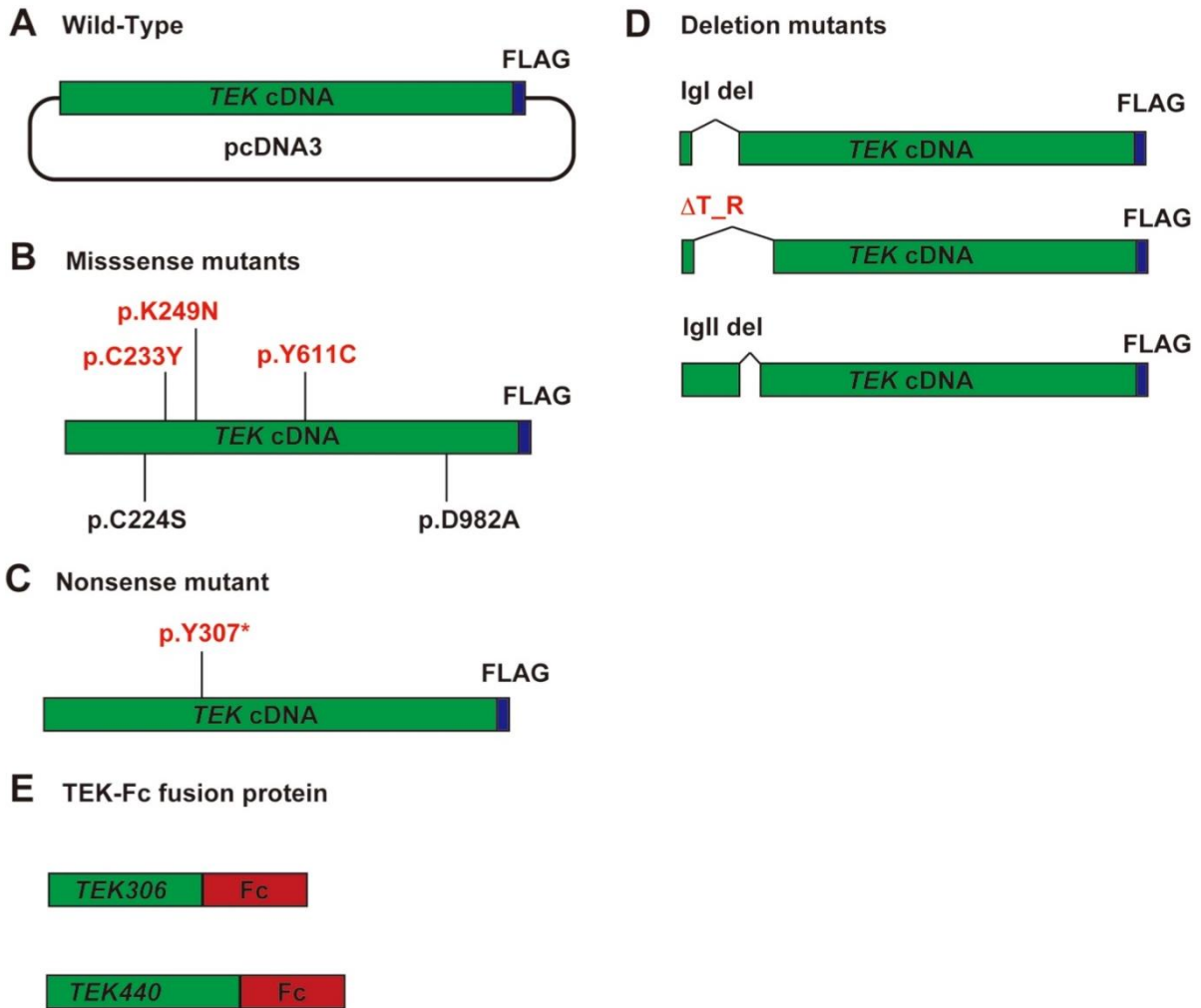
Ectodomain of TEK receptor (amino acid number 23-536, PDB ID: 4K0V (34)) with Angiopoietin1 (ANGPT1) is shown using YASARA (19). C233 and C224 form a disulfide bond (red) and create the loop structure in the EGF1 domain (cyan).



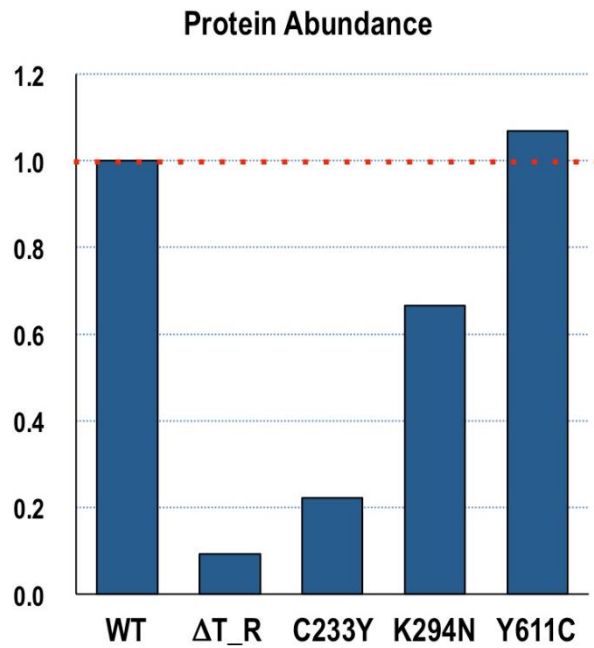
Supplemental Figure 5. FoldX result of the three missense variants. (A-B) FoldX results of p.C233Y and p.K294N using the known human TEK crystal structure (PDB ID: 2GY5 (15)). The p.C233Y mutation was predicted to be highly destabilizing to the protein structure (average ddG = 7.52 kcal/mol, SD=3.48) due to the loss of a disulfide bond with C224. (C) Fold X result of p.Y611C. A structural model of the TEK FN3 domain was created. FoldX predicted Y611C to be moderately destabilizing with an average ddG of 2.02 kcal/mol, SD=0.02. ddG =the difference in the calculated free energies between mutant and wild-type proteins. Blue, wild-type residues; Red, mutant residues; Yellow, hydrogen bonds.



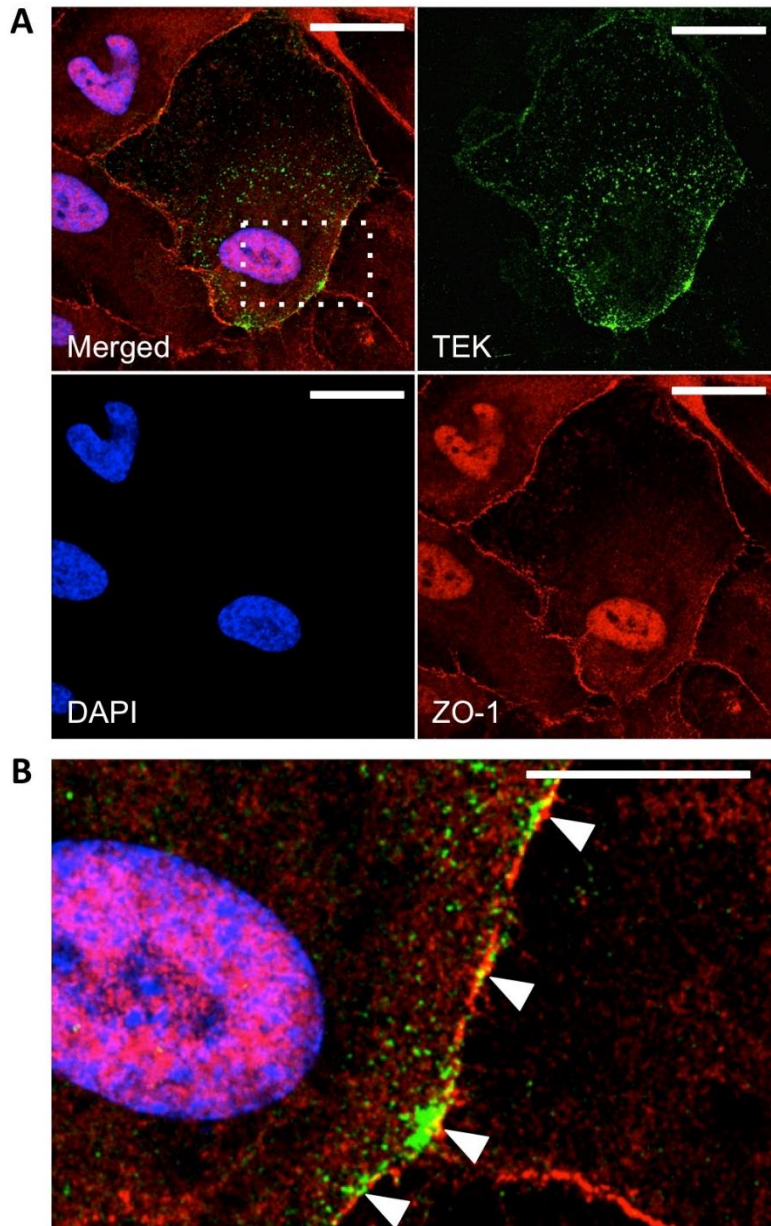
Supplemental Figure 6. TEK and TIE1 protein sequence conservation. Subfamily-specific conservation for regions containing variant residues p.C233, p.K294 and p.Y611. Orthologs for TEK are shown above paralogs for TIE1. The variant positions are shown at the bottom of each panel. Histograms show the degree of conservation at each residue.



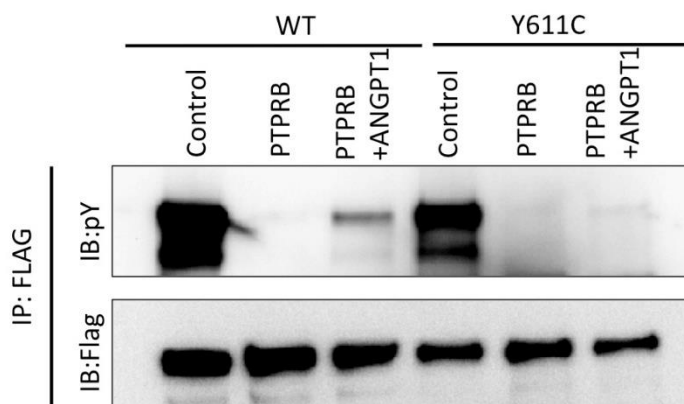
Supplemental Figure 7. Schematic representation of TEK plasmids structures. (A) Wild-type TEK expressing vector. Wild type TEK cDNA was cloned into the pcDNA3 vector with C-tail FLAG tag. (B) Missense mutants. Site-directed mutagenesis was performed to produce each mutant using the wild-type TEK-Flag expressing vector as template. (C) Nonsense mutant. The premature stop codon was introduced before the FLAG tag. (D) Deletion mutants. (E) TEK-Fc fusion proteins. TEK cDNA encoding 306 or 440 amino acids were directly fused to the Fc-tag cDNA, and cloned into the pcDNA3 vector. Please note that mutants in red are the PCG mutants.



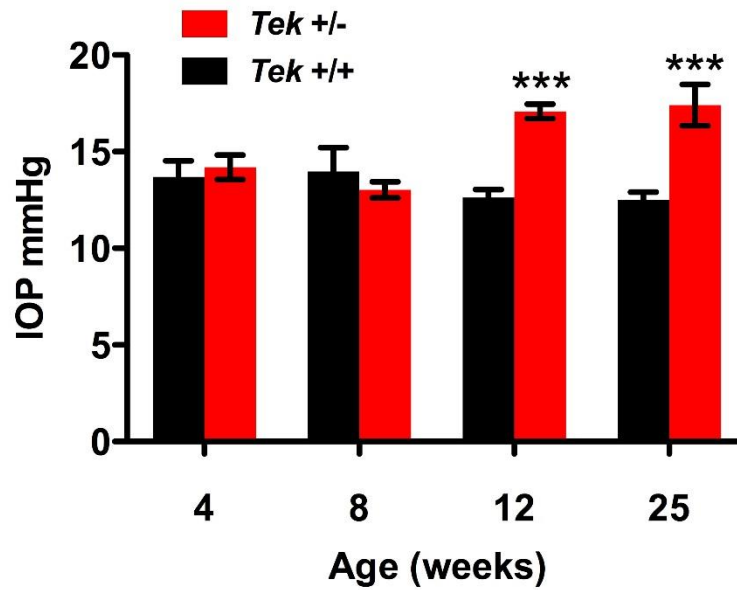
Supplemental Figure 8. Overall protein expression by stable isotope labeling by amino acids in cell culture (SILAC) analysis. Consistent with the immunoblotting results, we observed markedly reduced expression of the large deletion mutant (p.T19_R210del, labeled as Δ T_R) and p.C233Y mutant. Expression levels of p.Y611C were equivalent to wild-type (WT).



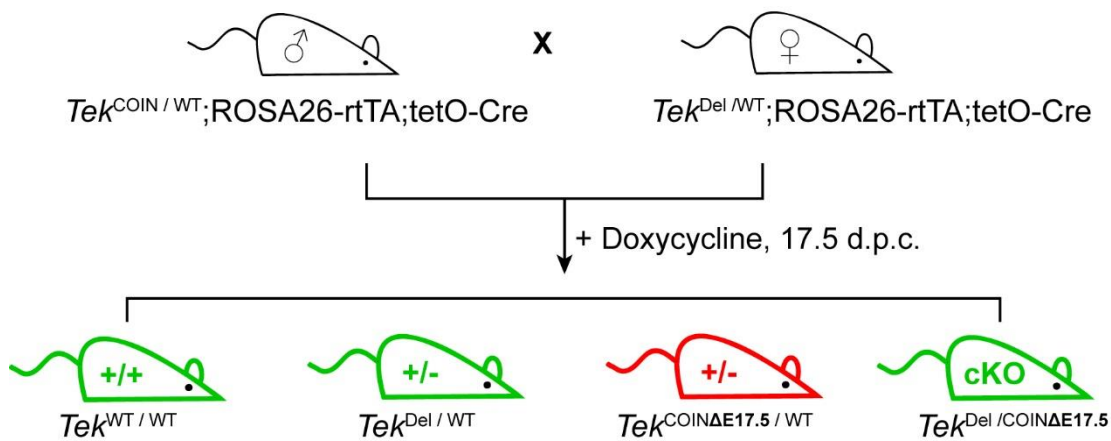
Supplemental Figure 9. ANGPT1 re-localizes TEK into cellular junctions. (A) Expression pattern of wild-type TEK in HUVEC with ANGPT1 stimulation. Transfected HUVEC cells were treated with ANGPT1 (600 ng/mL) for 30 min. The cells were fixed and stained with anti-Flag (green) and anti-ZO-1 antibody (red). Nuclei were stained with DAPI, 4',6-Diamidino-2-phenylindole dihydrochloride (blue). (B) Magnified image of dotted box in (A). White arrowheads indicate the TEK receptor on cellular junctions. Scale bars indicate 25 μ m in (A) and 10 μ m in (B). Data representative of more than 3 biological replicates are shown.



Supplemental Figure 10. p.Y611C mutant has reduced ligand responsiveness. Western blot analysis of wild type and p.Y611C mutant TEK proteins following immunoprecipitation with anti-Flag antibody. TEK proteins were co-expressed with protein tyrosine phosphatase receptor type B (PTPRB) in HEK293 cells, and stimulated with Angiopoietin 1 (ANGPT1) ligand, a major agonist of TEK receptor, (400 ng/mL) for 30 min at 37°C. Note that PTPRB completely abolished the phosphorylation of TEK proteins, and ANGPT1 stimulation recovers phosphorylation only in WT TEK. Data representative of 2 biological replicates are shown.



Supplemental Figure 11. Time-course analysis of intraocular pressure (IOP) change. IOP of control (*Tek+/+*) and *Tek* hemizygous (*Tek+/-*) mice were serially measured using a rebound tonometer (n=6-11). Please note that IOP levels of *Tek+/-* mice started to increase from 12 weeks old. *** $p < 0.001$. Two-way ANOVA with Bonferroni correction was used for statistical analysis.



Supplemental Figure 12. Breeding strategy of mouse models. *Tek* COIN (Conditional by inversion) mice were bred with whole body inducible Cre expressing mice (*ROSA26-rtTA*; *tetO-Cre*). The *ROSA26-rtTA-TetOnCre* system allowed robust, whole-body deletion of *Tek* upon induction with doxycycline. $Tek^{COIN\Delta E17.5 / WT}$ mice were excluded from the study population.

Supplemental Table 1. Primers for gDNA PCR amplification and direct Sanger sequencing of the human *TEK* gene core promoter region and coding exons.

Exon #	Forward Primer Sequence	Reverse Primer Sequence
Promoter	CCAACCAACAGGCCAT	GAGGAATTTTTGTTGG
1	GTCTGAGAAGGATTGGTCATCA	CTGGAGACTCACAGAGAAATGG
2	TTGGATTTTGTCCAGTGGAAG	GAGACAGGCAAGATCGTCAAG
3	AGTGCCAGCCCTCATTTTC	GCCCACAAGACCACAATAGG
4	AAACCAGACAAGGAAGCAGG	TTTGCTTAAGAAGCCATGGTTAG
5	TTCACCATTGTCCACTGAATG	TAGATCCAGCAACGATGGC
6	AAAGAATTATGTATTTCAAGGGGTTG	GCAGTCCAGGTATATCCGATG
7	TTCCCTGGATTAATACTGGTTT	TCCCAACTTCTGGATGGAAA
8	CCCGGTGCATGACTTACTAAA	AGTTCCTCCAGGAGGCATATT
9	GACCTTTGCGTTTATGCCTC	CCCAAAGGTATTTTAGTGGTCG
10	GAACAATCACAAAACCTCAAAGC	GTAGAGGATTGAGGCAGGGAG
11	ATCGCAATAACAACAACCCC	CCTGGTCTTCCTTCCTCTTTC
12	GGACACTAATCCAACTATATCAGCC	GTTAGCTAAGTCTGCATGGCG
13	ACCAATTGATTGGGGTACCAT	CCTATAGGGCTGCACGGTAA
14	ACGGTGTGGGTCTGTTTCTC	AAGGTTCTGCCTGTACTTGGAC
15	ACCAGAAGACATTATGCCCC	AAATCAAGTTTTCTCCACACCC
16	TGGTGACTGAGGGTAGCTGA	CAAAAACAAGGCAAACCACA
17	AATGTCATAGCTGTTTCAGGGC	AACTGACTTTAGAGGGAACTCCAC
18	TGTTCCCCAAAGTTTTTCAGC	AGCAACATCAGGAGACAGGG
19	GAGCCTCTTAAAGACCCTGTCC	TTGTTCCCGAGAGCTACAGG
20	TCTCCCTGGCTTTTGGG	GAGGCTTCCACTCACTTTGC
21	TCACCCTCTCTTGCCATAACC	AAAATAGCCCCAGGATGAGG
22	CTCCTCTCTTTTCCTGCCG	CCTGGGCACATCAGGTATTC
23.1	GAAAAGTATCCCCAAGTGCT	CGCCTTCCTATGAAGTCCAC
23.2	AATCAGAATGCCTGTTTGTGG	AGGCTTGTAAGCAATGAGATTTAAG
23.3	TGAATGCTATTAATGTTTTCTGTG	CTGGAACACTCCCAAAGGTG

Supplemental Table 2. Mouse genotyping primer sequences.

Gene	Forward Primer Sequence	Reverse Primer Sequence
<i>Tek</i> ^{COIN}	CTGAAGCACTGCACGCCGTAG	CTCAGAGTATTTTATCCTCATCTC
<i>Tek</i> ^{COININV}	CTGAAGCACTGCACGCCGTAG	GTTTTCAGGGTGTGTTTAG
<i>Tek</i> ^{WT}	GCTCAGACAGAAATGAGACTG	GAATCTGAACTTCAAACCGTTGCCA
tetO-Cre	GTGCAAGTTGAATAACCGGAAATGG	AGAGTCATCCTTAGCGCCGTAAATCAAT
Rosa26-rtTA	GGCGAGTTTACGGGTTGTTA	AAGGGAGCTGCAGTGGAGTA

Supplemental references

1. Li H, and Durbin R. Fast and accurate short read alignment with Burrows-Wheeler transform. *Bioinformatics*. 2009;25(14):1754-60.
2. DePristo MA, Banks E, Poplin R, Garimella KV, Maguire JR, Hartl C, Philippakis AA, del Angel G, Rivas MA, Hanna M, et al. A framework for variation discovery and genotyping using next-generation DNA sequencing data. *Nat Genet*. 2011;43(5):491-8.
3. McKenna A, Hanna M, Banks E, Sivachenko A, Cibulskis K, Kernytsky A, Garimella K, Altshuler D, Gabriel S, Daly M, et al. The Genome Analysis Toolkit: a MapReduce framework for analyzing next-generation DNA sequencing data. *Genome research*. 2010;20(9):1297-303.
4. Wei Z, Wang W, Hu P, Lyon GJ, and Hakonarson H. SNVer: a statistical tool for variant calling in analysis of pooled or individual next-generation sequencing data. *Nucleic acids research*. 2011;39(19):e132.
5. Rimmer A, Phan H, Mathieson I, Iqbal Z, Twigg SR, Consortium WGS, Wilkie AO, McVean G, and Lunter G. Integrating mapping-, assembly- and haplotype-based approaches for calling variants in clinical sequencing applications. *Nat Genet*. 2014;46(8):912-8.
6. Wang K, Li M, and Hakonarson H. ANNOVAR: functional annotation of genetic variants from high-throughput sequencing data. *Nucleic acids research*. 2010;38(16):e164.
7. Adzhubei I, Jordan DM, and Sunyaev SR. Predicting functional effect of human missense mutations using PolyPhen-2. *Current protocols in human genetics / editorial board, Jonathan L Haines [et al]*. 2013;Chapter 7(Unit7 20).
8. Adzhubei IA, Schmidt S, Peshkin L, Ramensky VE, Gerasimova A, Bork P, Kondrashov AS, and Sunyaev SR. A method and server for predicting damaging missense mutations. *Nature methods*. 2010;7(4):248-9.
9. Sim NL, Kumar P, Hu J, Henikoff S, Schneider G, and Ng PC. SIFT web server: predicting effects of amino acid substitutions on proteins. *Nucleic acids research*. 2012;40(Web Server issue):W452-7.
10. Katoh K, and Toh H. Recent developments in the MAFFT multiple sequence alignment program. *Briefings in bioinformatics*. 2008;9(4):286-98.
11. Waterhouse AM, Procter JB, Martin DM, Clamp M, and Barton GJ. Jalview Version 2--a multiple sequence alignment editor and analysis workbench. *Bioinformatics*. 2009;25(9):1189-91.
12. Schneider G, Wildpaner M, Sirota FL, Maurer-Stroh S, Eisenhaber B, and Eisenhaber F. Integrated tools for biomolecular sequence-based function prediction as exemplified by the ANNOTATOR software environment. *Methods in molecular biology*. 2010;609(257-67).
13. Schymkowitz J, Borg J, Stricher F, Nys R, Rousseau F, and Serrano L. The FoldX web server: an online force field. *Nucleic acids research*. 2005;33(Web Server issue):W382-8.
14. Berman HM, Westbrook J, Feng Z, Gilliland G, Bhat TN, Weissig H, Shindyalov IN, and Bourne PE. The Protein Data Bank. *Nucleic acids research*. 2000;28(1):235-42.
15. Barton WA, Tzvetkova-Robev D, Miranda EP, Kolev MV, Rajashankar KR, Himanen JP, and Nikolov DB. Crystal structures of the Tie2 receptor ectodomain and the angiopoietin-2-Tie2 complex. *Nature structural & molecular biology*. 2006;13(6):524-32.
16. Kumar PR CA, Almo SC. Crystal structure of an internal FN3 domain from human

- Contactin-5 [PSI-NYSGRC-005804].
17. Webb B, and Sali A. Protein structure modeling with MODELLER. *Methods in molecular biology*. 2014;1137(1-15).
 18. Van Durme J, Delgado J, Stricher F, Serrano L, Schymkowitz J, and Rousseau F. A graphical interface for the FoldX forcefield. *Bioinformatics*. 2011;27(12):1711-2.
 19. Krieger E, and Vriend G. YASARA View - molecular graphics for all devices - from smartphones to workstations. *Bioinformatics*. 2014;30(20):2981-2.
 20. Luke RW, Ballard P, Buttar D, Campbell L, Curwen J, Emery SC, Griffen AM, Hassall L, Hayter BR, Jones CD, et al. Novel thienopyrimidine and thiazolopyrimidine kinase inhibitors with activity against Tie-2 in vitro and in vivo. *Bioorganic & medicinal chemistry letters*. 2009;19(23):6670-4.
 21. Desmet FO, Hamroun D, Lalande M, Collod-Beroud G, Claustres M, and Beroud C. Human Splicing Finder: an online bioinformatics tool to predict splicing signals. *Nucleic acids research*. 2009;37(9):e67.
 22. Faber K, Glatting KH, Mueller PJ, Risch A, and Hotz-Wagenblatt A. Genome-wide prediction of splice-modifying SNPs in human genes using a new analysis pipeline called AASsites. *BMC bioinformatics*. 2011;12 Suppl 4(S2).
 23. Fiedler U, Krissl T, Koidl S, Weiss C, Koblizek T, Deutsch U, Martiny-Baron G, Marme D, and Augustin HG. Angiopoietin-1 and angiopoietin-2 share the same binding domains in the Tie-2 receptor involving the first Ig-like loop and the epidermal growth factor-like repeats. *J Biol Chem*. 2003;278(3):1721-7.
 24. Ong SE, and Mann M. A practical recipe for stable isotope labeling by amino acids in cell culture (SILAC). *Nature protocols*. 2006;1(6):2650-60.
 25. Fukuhara S, Sako K, Minami T, Noda K, Kim HZ, Kodama T, Shibuya M, Takakura N, Koh GY, and Mochizuki N. Differential function of Tie2 at cell-cell contacts and cell-substratum contacts regulated by angiopoietin-1. *Nature cell biology*. 2008;10(5):513-26.
 26. Saharinen P, Eklund L, Miettinen J, Wirkkala R, Anisimov A, Winderlich M, Nottebaum A, Vestweber D, Deutsch U, Koh GY, et al. Angiopoietins assemble distinct Tie2 signalling complexes in endothelial cell-cell and cell-matrix contacts. *Nature cell biology*. 2008;10(5):527-37.
 27. Thomson BR, Heinen S, Jeansson M, Ghosh AK, Fatima A, Sung HK, Onay T, Chen H, Yamaguchi S, Economides AN, et al. A lymphatic defect causes ocular hypertension and glaucoma in mice. *J Clin Invest*. 2014;124(10):4320-4.
 28. John SW, Hagaman JR, MacTaggart TE, Peng L, and Smithes O. Intraocular pressure in inbred mouse strains. *Investigative ophthalmology & visual science*. 1997;38(1):249-53.
 29. McLean IW, and Nakane PK. Periodate-lysine-paraformaldehyde fixative. A new fixation for immunoelectron microscopy. *The journal of histochemistry and cytochemistry : official journal of the Histochemistry Society*. 1974;22(12):1077-83.
 30. Schindelin J, Arganda-Carreras I, Frise E, Kaynig V, Longair M, Pietzsch T, Preibisch S, Rueden C, Saalfeld S, Schmid B, et al. Fiji: an open-source platform for biological-image analysis. *Nature methods*. 2012;9(7):676-82.
 31. Smith RS, Sundberg JP, and John SWM. In: Smith RS, John SWM, Nishina PM, and Sundberg JP eds. *Systematic Evaluation of the Mouse Eye: Anatomy, Pathology and Biomethods*. Boca Raton: CRC Press; 2002:25-45.
 32. Smith RS, Zabaleta A, Kume T, Savinova OV, Kidson SH, Martin JE, Nishimura DY,

- Alward WL, Hogan BL, and John SW. Haploinsufficiency of the transcription factors FOXC1 and FOXC2 results in aberrant ocular development. *Hum Mol Genet.* 2000;9(7):1021-32.
33. Smith RS, Zabaleta A, Savinova OV, and John SW. The mouse anterior chamber angle and trabecular meshwork develop without cell death. *BMC Dev Biol.* 2001;1(3).
34. Yu X, Seegar TC, Dalton AC, Tzvetkova-Robev D, Goldgur Y, Rajashankar KR, Nikolov DB, and Barton WA. Structural basis for angiopoietin-1-mediated signaling initiation. *Proc Natl Acad Sci U S A.* 2013;110(18):7205-10.